

See discussions, stats, and author profiles for this publication at: <https://www.researchgate.net/publication/265019489>

ChemInform Abstract: pH-Controlled and Sulfite Anion-Directed Assembly of a Family of Cerium(III)-Containing Polyoxotungstates Clusters.

ARTICLE *in* CHEMINFORM · AUGUST 2014

Impact Factor: 0.74 · DOI: 10.1021/ic500442k · Source: PubMed

CITATIONS

10

READS

30

7 AUTHORS, INCLUDING:



Wei-Chao Chen

Northeast Normal University

9 PUBLICATIONS 46 CITATIONS

SEE PROFILE

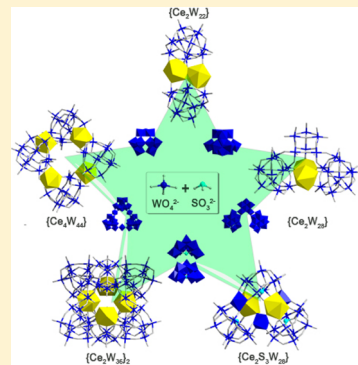
pH-Controlled and Sulfite Anion-Directed Assembly of a Family of Cerium(III)-Containing Polyoxotungstates Clusters

Wei-Chao Chen, Xin-Long Wang,* Yan-Qing Jiao, Peng Huang, En-Long Zhou, Zhong-Min Su,* and Kui-Zhan Shao

Department Institute of Functional Material Chemistry, Key Lab of Polyoxometalate Science of Ministry of Education, Department of Chemistry, Northeast Normal University, Changchun 130024, P. R. China

Supporting Information

ABSTRACT: A versatile one-pot strategy was employed to synthesize five cerium(III)-containing polyoxotungstate nanoclusters through pH-controlled and sulfite anion-directed assembly: $[C_2H_8N]_3Na_7[Ce_2(H_2O)_6W_{22}O_{72}(OH)_4] \cdot 20H_2O$ (**1**) at pH 5.0; $[C_2H_8N]_8Na_{16}[Ce_4(H_2O)_{12}W_{44}O_{144}(OH)_{12}] \cdot 23H_2O$ (**2**) at pH 4.5; $[C_2H_8N]_2Na_4Ce_2[Ce_2(H_2O)_{10}W_{28}O_{92}(OH)_2] \cdot 27H_2O$ (**3**) at pH 2.8–3.3; $[C_2H_8N]_2Na_7[\{\alpha-SW_7O_{28}\}\{Ce_2(H_2O)_6\}(W_3O_6)\{\alpha-SW_9O_{32}\}\{\alpha-SW_9O_{31}(OH)\}] \cdot 18H_2O$ (**4**) at pH 2.5; $[C_2H_8N]_2Na_{18}[Ce_2(H_2O)_9W_{36}O_{110}(OH)_{12}] \cdot 30H_2O$ (**5**) at pH 1.5. These compounds were characterized by single-crystal X-ray structure analysis, IR spectroscopy, thermogravimetric (TG) analysis, X-ray photoelectron spectroscopy (XPS), and electrospray ionization mass spectrometry (ESI-MS). Moreover, their electrochemical properties were investigated. Single-crystal X-ray structure analysis revealed that **1** and **2** were di- and tetra-cerium(III)-bridged polyoxotungstates, constructed from two different types of lacunary $\{W_{11}\}$ units. **3** composed of the well-known cerium(III)-stabilized $\{W_{28}\}$ unit and organic amine–sodium–cerium cations, was isolated in the pH range 2.8–3.3. In this reaction system, the SO_3^{2-} anion acted as a heteroanion template at a lower pH 2.5. **4** was isolated by the combination of cerium(III) centers and SO_3^{2-} heteroanion template, which is the first lanthanide-containing polyoxotungstates with sulfur heteroatoms, and the 4f metal cerium(III) centers in **4** both have eight-coordinated modes and the SO_3^{2-} heteroanion templates display μ_7 and μ_9 coordination modes. At a much lower pH 1.5, the polyanion of **5** was obtained, two triangular-shaped $\{W_{36}\}$ subunits were bridged by the cerium(III) ions, resulting in the largest lanthanide-containing iso-polyoxotungstates known to date.



INTRODUCTION

Polyoxometalates (POMs) constitute a large family of anionic clusters which can be viewed as soluble molecular oxides of early transition metals in high oxidation state (e.g., W^{VI} , $Mo^{V/VI}$, V^V , and Nb^V).¹ As a family of inorganic compounds, they possess an exceptional range of both structural and compositional diversity, allowing blending of their electronic structure as well as their potential functionality, including magnetism, multifunctional materials, nanotechnology, and so on.² Although the first POM had already been synthesized in 1826 by Berzelius,^{1a} the mechanism of POM formation is still not well-known.³ There are many factors affecting the self-assembly synthesis process (e.g., reaction temperature, ionic strength, pH values, mole ratio of the reactants, etc.), among which the suitable reaction pH ranges have already been proved to be a strong influence on the reaction pathways in solution.⁴ Moreover, the use of some inorganic anions (e.g., PO_4^{3-} , SO_3^{2-} , etc.), involving anion templates (e.g., PO_4^{3-} -mediated POM supercluster assembly)⁵ or anion control experiments that the anions do not exist in the final structure (e.g., the formations of $\{W_{22}\}$ and $\{W_{34}\}$ isopolyoxotungstate clusters),⁶ also constitutes a key feature in the formation of POMs.⁷ Therefore, understanding the role of anion-directed assembly

process remains an important research subject to allow for a prospective design of tailored POM assemblies.

Lanthanide (Ln)-containing polyoxotungstates (POTs), especially the iso- and hetero-POTs fragments bridged or stabilized by the Ln centers, establish one of the most-interesting subgroups ascribed to its photoluminescence, catalytic, electrochemical, and magnetic properties.⁸ In recent years, there is a significant increase of Ln-containing hetero-POTs to be reported.^{8a} The large sizes of Ln centers accompanied by their high coordination numbers (usually 8–12) trend to link or stabilize the lacunary POTs building blocks, such as $[As_2W_{19}O_{67}(H_2O)]^{14-}$, $[\alpha-GeW_9O_{34}]^{10-}$, $[\alpha-P_2W_{15}O_{56}]^{12-}$, $[\beta_2-SiW_{11}O_{39}]^{8-}$, etc.⁹ In this respect, lacunary hetero-POTs building blocks are particularly important because they can be used as multidentate ligands to construct much larger nanoscale Ln-containing hetero-POTs. Most recent reports on lacunary hetero-POTs are mainly based upon the heteroanion templates (e.g., AsO_3^{3-} , GeO_4^{4-} , PO_4^{3-} , SiO_4^{4-} , SbO_3^{3-} , BiO_3^{3-}),⁹ a detailed survey of the heteroatom-based Ln-containing hetero-POTs is given in Table S1 in the Supporting Information. Recently, our group also reported a

Received: February 27, 2014

Published: August 25, 2014

Table 1. Detailed Survey of Lanthanide-Containing Isopolyoxotungstates

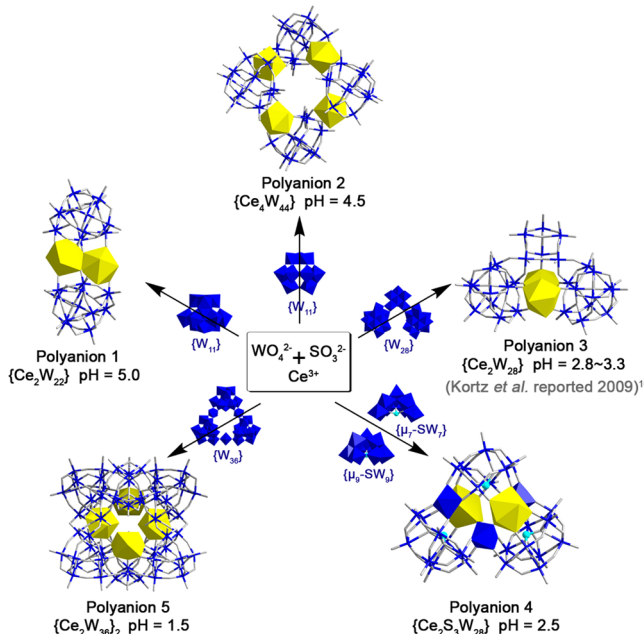
year	formula	pH	T (°C)	Tungsten centers type ^a (mW _n)	ref
1971–1974	[Ln(W ₅ O ₁₈) ₂] ⁿ⁻ (Ln = La, Ce ³⁺ , Ce ⁴⁺ , Pr, Nd, Sm, Ho or Yb)	6.5–7.5	85	2W ₅	13
2008	[H ₆ Ce ₂ (H ₂ O)Cl(W ₅ O ₁₈) ₃] ⁷⁻	5.0	100	3W ₅	14
2009	[Ln ₂ (H ₂ O) ₁₀ W ₂₂ O ₇₁ (OH) ₂] ⁸⁻ (Ln = La, Ce, Tb, Dy, Ho, Er, Tm, Yb, or Lu)	2.2	R.T.	W ₂₂	15
2009	[Ln ₂ (H ₂ O) ₁₀ W ₂₈ O ₉₃ (OH) ₂] ¹⁴⁻ (Ln = Sm or Eu)	3.2	R.T.	2W ₁₁ + W ₆	16
2013	[Ln ₄ (WO ₄)(H ₂ O) ₁₆ {W ₇ O ₂₂ (O ₂) ₂ } ₄] ¹⁴⁻ (Ln = La or Pr)	3.0	R.T.	4W ₇	17
2014	[Ce ₂ (H ₂ O) ₆ W ₂₂ O ₇₂ (OH) ₄] ¹⁰⁻	5.0	70	2W ₁₁	this work
2014	[Ce ₄ (H ₂ O) ₁₂ W ₄₄ O ₁₄₄ (OH) ₁₂] ²⁴⁻	4.5	70	4W ₁₁	this work
2014	[Ce ₂ (H ₂ O) ₉ W ₃₆ O ₁₁₀ (OH) ₁₂] ²⁰⁻	1.5	70	W ₃₆	this work

^am and n refer to the number of different tungsten building blocks within a polyanion and the number of tungsten centers within a unit, respectively.

series of Ln-containing hetero-POTs by combining cerium linkers with SeO₃²⁻ or TeO₃²⁻ heteroanion templates.¹⁰ However, the tungsten pyramidal sulfite ion (SO₃²⁻) system remains explored less up to date, only the Dawson-type {W₁₈} cages incorporating the targeted one or two pyramidal sulfite ions as the central cluster templates were reported by Cronin et al.^{7,11}

Because only a few iso-POTs building blocks have been isolated, including [HW₅O₁₉]⁷⁻, [H₄W₁₁O₃₈]⁶⁻, [H₂W₁₂O₄₀]⁶⁻, [H₂W₁₂O₄₂]¹⁰⁻, [H₄W₂₂O₇₄]¹²⁻, and [H₁₂W₃₆O₁₂₀]¹²⁻,^{6,12} the interactions of Ln ions with iso-POTs have been studied less than hetero-POTs. Kortz et al. have reviewed this field in a comprehensive fashion recently;^{8a} meanwhile, many other groups have also paid much attention to this field.^{13–17} As shown in Table 1, the classical Lindqvist sandwich-type structures (synthesized at pH 5.0–7.0) have been studied early years,¹³ whereafter, Cao and co-workers reported a pentadecatungstate [H₆Ce₂(H₂O)Cl(W₅O₁₈)₃]⁷⁻ consisting of dinuclear cerium(III) centers and the {W₅} units, which was obtained in a weakly acidic medium at pH 5.0.¹⁴ In 2009, Kortz and co-workers synthesized the polyanions [Ln₂(H₂O)₁₀W₂₂O₇₁(OH)₂]⁸⁻ (Ln = La, Ce, Tb, Dy, Ho, Er, Tm, Yb, and Lu) based on the {W₂₂} building blocks¹⁵ and the “V”-shaped polyanions [Ln₂(H₂O)₁₀W₂₈O₉₃(OH)₂]¹⁴⁻ (Ln = Sm, and Eu) based on the {W₁₁} units by the reaction of WO₄²⁻ and Ln ions in acidic aqueous medium with pH 2.0–3.5.¹⁶ Recently, Niu and co-workers discovered Ln-containing peroxyisopolytungstate [Ln₄(WO₄)(H₂O)₁₆{W₇O₂₂(O₂)₂}₄]¹⁴⁻ (Ln = Sm, and Eu) involving the [W₇O₂₂(O₂)₂]⁶⁻ units with tetrahedral WO₄²⁻ template cores in an acidic medium at pH 3.0, which remains the largest tungsten nuclearities ever seen in Ln-containing iso-POTs.¹⁷

The sulfite anion has a C_{3v} symmetry and contains a nonbonding but stereochemically active pair of electrons, also observed in SeO₃²⁻ or TeO₃²⁻ heteroanions,¹⁸ which may be beneficial for exploring the sulfite anion-directed assembly of Ln-containing iso-POTs.⁷ Therefore, it may be a meaningful synthesis strategy to combine the pH-controlled and {SO₃²⁻}-directed assembly strategy along with cerium(III) centers to discover new members of the Ln-containing POTs family. Here, five cerium(III)-containing POTs have been isolated depending on the pH values by using this synthesis strategy (Scheme 1): [C₂H₈N]₃Na₇[Ce₂(H₂O)₆W₂₂O₇₂(OH)₄]·20H₂O (**1**) at pH 5.0; [C₂H₈N]₈Na₁₆[Ce₄(H₂O)₁₂W₄₄O₁₄₄(OH)₁₂]·23H₂O (**2**) at pH 4.5; [C₂H₈N]₂Na₄Ce₂[Ce₂(H₂O)₁₀W₂₈O₉₂(OH)₂]₂·27H₂O (**3**) at pH 2.8–3.3; [C₂H₈N]₂Na₇[{ α -SW₇O₂₈}·{Ce₂(H₂O)₆}·(W₃O₆)₂·{ α -SW₉O₃₂}·{ α -SW₉O₃₁(OH)}]₂·18H₂O (**4**) at pH 2.5; [C₂H₈N]₂Na₁₈[Ce₂(H₂O)₉W₃₆O₁₁₀(OH)₁₂]₂·30H₂O (**5**) at pH 1.5. Single-crystal X-ray

Scheme 1. Synthetic Procedure of **1–5**

structure analysis revealed that two different types of lacunary {W₁₁} units existing in **1** or **2** constituted the di-, or tetracerium(III)-bridged POTs. The polyanion of **3** was obtained at the pH range from 2.8 to 3.3, which has the similar configuration as Kortz et al. reported in 2009, but SO₃²⁻ anion and organic amine-sodium–cerium counter cations were employed during the assembly.¹⁶ The assembly and isolation of **4** was based on the combination of cerium(III) centers and SO₃²⁻ heteroanion template at pH 2.5, which remains the first Ln-containing POTs with sulfur heteroatom. The cerium(III) centers in **4** are eight-coordinated and the SO₃²⁻ heteroanion templates display μ_7 and μ_9 coordination modes. The polyanion of **5** was obtained at much lower pH of 1.5, in which the cerium(III) centers were bridged by two triangular-shaped {W₃₆}^{12f} units, resulting in the largest Ln-containing iso-POTs. The polyanions of **1–5** can be isolated in good yields only by using Na₂SO₃, which has been verified by a series of parallel experiments.

EXPERIMENTAL SECTION

General Considerations. All commercially obtained reagent, including Na₂WO₄·2H₂O, Na₂SO₃, acetic acid, Ce(NO₃)₃·6H₂O, dimethylamine hydrochloride, HCl, were purchased from Aldrich and used without further purification. Deionized water was used throughout the study. The reaction mixtures were heated and agitated

in the round bottomed flasks with reflux condensing tubes on a CL-1A-type agitator purchased from GongYi Company in China. A pH-S-2B pH meter was used for pH measurements.

Synthesis of $[C_2H_8N]_3Na_2[Ce_2(H_2O)_6W_{22}O_{72}(OH)_4]\cdot20H_2O$ (1). $Na_2WO_4\cdot2H_2O$ (3.00 g, 9.09 mmol) and Na_2SO_3 (0.20 g, 1.58 mmol) were dissolved in 40 mL of water. The pH of the solution was adjusted to 5.5 with 50% acetic acid solution, and the reaction mixture was stirred for 60 min. Solid $Ce(NO_3)_3\cdot6H_2O$ (0.43 g, 1.00 mmol) and dimethylamine hydrochloride (1 g, 12.26 mmol) were successively added. The final pH was kept at 5.0 by adjustment with 4 M HCl. This solution was heated to 70 °C stirred for 1 h, and then cooled to room temperature and filtered. After slow evaporation at about 10 °C for about two months, yellow block-shaped crystals were obtained, which were then collected by filtration and air-dried. Yield: 0.73 g (28% based on W). IR (KBr disk (see Figure S20 in the Supporting Information)) ν/cm^{-1} : 3421(w), 3144(w), 2783(w), 1620(s), 1469(s), 946(s), 886(s), 804(w), 746(m). Elemental anal. Calcd (%) (found): C 1.14 (1.10), H 1.28 (1.25), N 0.67 (0.70), Na 2.55 (2.49), W 64.07 (64.30), Ce 4.44 (4.51).

Synthesis of $[C_2H_8N]_8Na_{16}[Ce_4(H_2O)_{12}W_{44}O_{144}(OH)_{12}]\cdot23H_2O$ (2). The synthesis process of 2 is similar to 1, but the pH of the solution was adjusted to 4.5 by the addition of aqueous 4 M HCl before heating to 70 °C. After slow evaporation at about 10 °C for about one month, yellow block-shaped crystals were obtained, which were then collected by filtration and air-dried. Yield: 0.49 g (19% based on W). IR (KBr disk (see Figure S21 in the Supporting Information)) ν/cm^{-1} : 3413(w), 3126(w), 2793(w), 1623(s), 1468(s), 973(s), 873(w), 763(s), 684(m). Elemental anal. Calcd (%) (found): C 1.53 (1.55), H 1.17 (1.21), N 0.89 (0.91), Na 2.94 (2.90), W 64.59 (64.61), Ce 4.47 (4.50).

Synthesis of $[C_2H_8N]_2Na_4Ce_2[Ce_2(H_2O)_{10}W_{28}O_{92}(OH)_2]\cdot27H_2O$ (3). The synthesis process of 3 is similar to 1, but the pH of the solution was adjusted to 2.8–3.3 by the addition of aqueous 4 M HCl before heating to 70 °C. After slow evaporation at about 10 °C for about two months, yellow block-shaped crystals were obtained, which were then collected by filtration and air-dried. Yield: 0.60 g (23% based on W). Elemental anal. Calcd (%) (found): C 0.60 (0.62), H 1.15 (1.17), N 0.35 (0.38), Na 1.14 (1.10), W 63.83 (63.87), Ce 6.95 (7.01).

Synthesis of $[C_2H_8N]_2Na_2[\{\alpha-SW_7O_{28}\}\{Ce_2(H_2O)_6\}\{W_3O_6\}\{\alpha-SW_9O_{32}\}\{\alpha-SW_9O_{31}(OH)\}]\cdot18H_2O$ (4). The synthesis process of 4 is similar to 1, but the pH of the solution was adjusted to 2.5 by the addition of aqueous 4 M HCl before heating to 70 °C. After slow evaporation at about 10 °C for about three months, orange block-shaped crystals were obtained, which were then collected by filtration and air-dried. Yield: 0.38 g (15% based on W). IR (KBr disk (see Figure S22 in the Supporting Information)) ν/cm^{-1} : 3432(w), 3148(w), 2777(w), 1638(s), 1463(s), 969(w), 888(s), 788(w), 723(m). Elemental anal. Calcd (%) (found): C 0.62 (0.60), H 0.84 (0.91), N 0.36 (0.29), Na 2.07 (2.04), S 1.24 (1.28), W 66.18 (66.20), Ce 3.60 (3.62).

Synthesis of $[C_2H_8N]_2Na_{18}[Ce_2(H_2O)_9W_{36}O_{110}(OH)_{12}]\cdot30H_2O$ (5). The synthesis process of 4 is similar to 1, but the pH of the solution was adjusted to 1.5 by the addition of aqueous 4 M HCl before heating to 70 °C. After slow evaporation at about 10 °C for about 2 months, yellow needle-shaped crystals were obtained, which were then collected by filtration and air-dried. Yield: 0.29 g (12% based on W). IR (KBr disk (see Figure S23 in the Supporting Information)) ν/cm^{-1} : 3428(w), 3121(w), 2781(w), 1615(s), 1463(s), 948(s), 893(w), 806(m), 769(m). Elemental anal. Calcd (%) (found): C 0.25 (0.30), H 0.72 (0.75), N 0.15 (0.18), Na 2.17 (2.12), W 69.32 (69.52), Ce 2.94 (3.01).

Characterization. Elemental analysis of Na, S, W, and Ce were performed with a Leaman inductively coupled plasma (ICP) spectrometer; C, H and N were performed on a PerkinElmer 2400 CHN elemental analyzer. IR spectra were recorded on an Alpha Centauri FTIR spectrophotometer on pressed KBr pellets in the range 400–4000 cm^{-1} . Water contents were determined by TG analyses on a PerkinElmer TGA7 instrument in flowing N_2 with a heating rate of 10 °C min^{-1} . XRD studies were performed with a Rigaku D/max-IBX X-ray diffractometer at a scanning rate of 1° min^{-1} with $Cu_K\alpha$ radiation

($\lambda = 1.5418 \text{ \AA}$). X-ray photoelectron spectroscopy was performed on a VG ESCALABMKII spectrometer with an $Mg_K\alpha$ (1253.6 eV) achromatic X-ray source. The vacuum inside the analysis chamber was maintained at 6.2×10^{-6} Pa during the analysis. Electrospray ionization mass spectrometry was carried out on a Bruker Micro TOF-QII instrument, the solutions of the investigated systems were prepared in water (1 mg/mL).

Single-Crystal X-ray Diffraction. Single-crystal X-ray diffraction data for 1–5 were recorded on a Bruker Apex CCD II area-detector diffractometer with graphite-monochromated $Mo_K\alpha$ radiation ($\lambda = 0.71073 \text{ \AA}$) at 296(2) K. Absorption corrections were applied using multiscan technique and performed by using the SADABS program.^{19a} The structures of 1–5 was solved by direct methods and refined on F^2 by full-matrix leastsquares methods by using the SHELXTL package.^{19b} Anisotropic thermal parameters were used to refine all non-hydrogen atoms. Hydrogen atoms attached to lattice water molecules were not located. The numbers of lattice water molecules and counter cations for 1–5 were estimated by the results of elemental analyses, TG curves, and calculations of electron count in the voids with SQEEZE.^{19c} CCDC 975840 (1), 975841 (2), 975842 (3), 975843 (4), and 975844 (5) contain the supplementary crystallographic data for this paper.

Electrochemical Experiments. Electrochemical measurements were carried out on a CHI 660 electrochemical workstation at room temperature. Thrice-distilled water was used throughout the experiments. All solutions were deaerated by bubbling high pure argon prior to the experiments and the electrochemical cell was kept under an argon atmosphere throughout the experiment. A conventional three-electrode system was used with a 1.5 mm glassy carbon working electrode, an Ag/AgCl reference electrode used as electrode, and a platinum wire counterelectrode. The glassy carbon working electrodes were polished with alumina on polishing pads, rinsed with distilled water, and sonicated in H_2O before each experiment. The scan rate was 30–500 mV s^{-1} . All potentials were measured and reported versus Ag/AgCl. Solutions 1–5 in 0.5 M H_2SO_4/Na_2SO_4 were used. A pH-S-2B pH meter was used for pH measurements.

RESULTS AND DISCUSSION

Synthesis. Compounds 1–5 were all synthesized using one-pot procedure by reaction of Na_2WO_4 and Na_2SO_3 with the pH range from 1.5–5.0 and isolated as mixed sodium–organic amine salts. The successful synthesis of 1–5 may be ascribed to the strategy of pH-controlled and sulfite anion-directed assembly with Ce^{III} ions.

First, it is worth noting that the directive functions of SO_3^{2-} anion in the assembly process. The ability of the sulfite anion to act as a template or anion control experiments, although it does not exist in the final structure, has been demonstrated in the case of molybdenum, tungsten and vanadium systems, which possess the inherent ability to form POM structures.⁷

Compound 4 seems to be a unique example of sulfur-containing POT cluster in terms of the SO_3^{2-} anion as structure-directing templates compared to the other four clusters. Anion template has emerged as a valuable tool for constructing a wide variety of significant assemblies in POMs,^{5,20} especially for the redox-inactive “conventional” heteroanion templates (e.g., SiO_4^{4-} , PO_4^{3-} , AsO_4^{3-}), most of the previous reports on lacunary hetero-POTs are based upon them. Recently, the redox active heteroanions from group VIA (e.g., SO_3^{2-} , SeO_3^{2-} , TeO_3^{2-}) have received much attention in an effort to engineer clusters with intrinsically more diverse structures, for example, assembly of molecular “layered” Hetero-POT architectures based on TeO_3^{2-} anion templates,^{18d} assembly of gigantic nanoscale Hetero-POTs by using SeO_3^{2-} as a template linker.^{18e} In this stage, SO_3^{2-} anion remains less developed in templating POTs system, only the

Table 2. Survey of the Sulfite Anion (μ_7 - or μ_9 -Coordination Modes) as a Template in POMs

year	formula	pH	T (°C)	template modes	ref
2004	[Mo ₁₈ O ₅₄ (SO ₃) ₂] ⁶⁻	~4.0	reflux	μ_9	21a
2005	[W ^{VI} ₁₈ O ₅₄ (SO ₃) ₂] ⁴⁻ [W ^{VI} ₁₈ O ₅₆ (SO ₃) ₂ (H ₂ O) ₂] ⁸⁻	1.9	reflux	μ_7, μ_9	11a
2008	[Mo ^{VI} ₁₁ V ^V ₅ V ^{IV} ₂ O ₅₂ (μ_9 -SO ₃)] ⁷⁻	3.0	R.T.	μ_9	21b
2010	[Mo ^{VI} ₁₁ V ^V ₅ V ^{IV} ₂ O ₅₂ (μ_9 -SO ₃)(Mo ^{VI} ₆ V ^{VO₂₂)]¹⁰⁻}	2.0–4.0	R.T.	μ_9	21c
2010	[H ₂ W ₁₈ O ₅₇ (SO ₃)] ⁶⁻ [W ₁₈ O ₅₆ (SO ₃) ₂ (H ₂ O) ₂] ⁸⁻	1.7	R.T.	μ_9	11b
2014	[Ce ₂ S ₃ W ₂₈ O ₉₇ (H ₂ O) ₆ (OH)] ⁹⁻	2.5	70	μ_7, μ_9	this work

Table 3. Crystal Data and Structure Refinements for 1–5

	1	2	3	4	5
empirical formula	C ₆ H ₈₀ Ce ₂ N ₃ Na ₇ O ₁₀₂ W ₂₂	C ₁₆ H ₁₄₆ Ce ₄ N ₈ Na ₁₆ O ₁₉₁ W ₄₄	C ₄ H ₉₂ Ce ₄ N ₂ Na ₄ O ₁₃₁ W ₂₈	C ₄ H ₆₅ Ce ₂ N ₂ Na ₇ O ₁₂₂ S ₃ W ₂₈	C ₄ H ₁₃₆ Ce ₄ N ₂ Na ₁₈ O ₂₉₂ W ₇₂
M	6312.60	12525.13	8065.04	7778.73	19096.65
λ (Å)	0.71073 Å	0.71073 Å	0.71073 Å	0.71073 Å	0.71073 Å
T (K)	296(2)	296(2)	296(2)	296(2)	296(2)
cryst syst	monoclinic	tetragonal	triclinic	triclinic	triclinic
space group	C2/c	I ₄ /a	P <bar{1}< td=""><td>P<bar{1}< td=""><td>P<bar{1}< td=""></bar{1}<></td></bar{1}<></td></bar{1}<>	P <bar{1}< td=""><td>P<bar{1}< td=""></bar{1}<></td></bar{1}<>	P <bar{1}< td=""></bar{1}<>
a (Å)	71.433(9)	25.987(4)	19.3210(17)	15.929(2)	17.8782(10)
b (Å)	12.8889(16)	25.987(4)	21.8489(19)	16.781(2)	23.3128(12)
c (Å)	38.595(5)	34.162(6)	22.0152(19)	27.229(4)	23.6398(13)
α (deg)	90	90	72.2390(10)	78.097(2)	70.4370(10)
β (deg)	105.632(3)	90	69.4860(10)	79.359(2)	80.1970(10)
γ (deg)	90	90	86.8980(10)	65.014(2)	77.0890(10)
V (Å ³)	34219(7)	23071(6)	8274.8(12)	6416.3(15)	9000.4(8)
Z	12	4	2	2	1
D_c (Mg m ⁻³)	3.676	3.606	3.237	4.026	3.523
μ (mm ⁻¹)	23.020	22.735	20.546	25.856	23.503
F(000)	34776	21960	7052	6784	8268
θ range (deg)	1.72–25.00	1.85–25.00	1.78–25.00	1.90–25.00	1.79–23.75
measd reflns	87931	58962	43391	33508	42529
ind reflns	30112	10158	28765	22278	27247
data/restraints/params	30112/319/1662	10158/290/614	28765/325/1594	22278/967/1351	27247/479/1720
R_{int} after SQUEEZE	0.0693	0.1201	0.0442	0.0588	0.0588
GOF on F^2	0.947	1.030	0.924	1.000	0.915
$R_1(I > 2\sigma(I))^a$	0.0404	0.0448	0.0484	0.0708	0.0531
wR ₂ (all data) ^b	0.0939	0.0949	0.1105	0.1806	0.1176

$$^a R_1 = \sum |F_0| - |F_c| / \sum |F_0|. \quad ^b wR_2 = \{\sum [w(F_0^2 - F_c^2)^2] / \sum [w(F_0^2)]\}^{1/2}.$$

Dawson-type {W₁₈} cages incorporating the targeted one or two pyramidal sulfite ions as the central cluster templates were reported.^{7,11} The pyramidal SO₃²⁻ anion as structure-directing template with its lone pair of electrons, reducing agent as well as inorganic ligand, introduces the necessary diversity into POM systems and allows access to new libraries of building blocks and then controls the associated assembly process.⁷ As for 4, two tips should be mentioned during the synthesis: (i) the formation of lacunary Keggin-type { α -SW₇} and { α -SW₉} units. The SO₃²⁻ anion reveals a multiple set of coordination modes, such as commonly μ_3 , μ_4 , μ_5 , μ_6 , μ_7 or μ_9 etc. The initial driving force is attributed to the electrophilicity of the POT-based building units and the nucleophilicity of the sulfite anions combined with their various ability of coordination (μ_7 for { α -SW₇} and μ_9 for { α -SW₉}) to act as inorganic ligands, in other words, the POT species “grow” around the pyramidal SO₃²⁻ anion which effectively prevents the “closure” of the POT assemblies to the Keggin-type cluster, and instead gives rise to “open” lacunary units, as the Keggin-type { α -SW₇} and { α -SW₉} units in 4. Moreover, the use of bulky “shrink-wrapping” cations, namely protonated organic amine cations (dimethylamine hydrochloride), restricts and stabilizes low-symmetry clusters that can be used as building blocks: Keggin-type { α -

SW₇} and { α -SW₉} units. There were no clusters to be isolated using other different counterions (for example, potassium or cesium etc.) in the reactions. (ii) the existence of the Ce centers. 4f Ce ions display a powerful ability to link lacunary POTs to build unprecedented architectures because of its oxophilicity and high coordination numbers. The larger size of Ce ions prevents its full incorporation in lacunary frameworks as addendum atoms, and therefore additional sites are available for further derivatization. Thus, the combination of Ce centers and the sulfite anion templates with its structural diversity is beneficial for obtaining novel sulfur-containing POT clusters.

The SO₃²⁻ anion acts as anion control experiments during the synthesis of 1, 2, 3, and 5, although it does not exist in the final structure. A series of anion control experiments have been carried out without sulfite, there are no products obtained except the classical {W₁₂} iso-POT fragment.^{6,18b} Furthermore, if sulfite was substituted by other anions, such as the sulfate, dithionate, silicate, nitrate, bismuthate, or phosphate under the same reaction conditions, there are still no compounds to be isolated.

Second, pH-controlled synthesis is the other fundamental factor in the reaction system (Scheme 1). Precise pH control of the one-pot reaction conditions was employed for the assembly

of **1–5**. At pH 5.0 with the existence of SO_3^{2-} simultaneously, **1** was obtained. During the synthesis of **2**, the pH was adjusted to about 4.5 and also with sulfite anion-directed assembly. Polyanion of **3** was obtained at the pH range from 2.8 to 3.3 with a similar configuration as Kortz et al. reported in 2009 (Scheme 1),¹⁶ but there are two differences during the synthesis of **3**, including the use of sulfite and the extra dimethylamine cations. **4** with the SO_3^{2-} anion as a template was isolated as a mixed sodium-organic amine salt at a lower pH 2.5, and **5** was obtained at the lowest pH 1.5. It is worth noting that SO_3^{2-} anion is always found to act as a template in the synthesis of POMs at a low pH values (generally pH < 4.0 and even pH < 2.0) according to many other works.^{11,21} It acts as templates usually showing μ_7 - or μ_9 -coordination modes in cage-type POMs (Table 2) at low pH values and even pH < 2.0 in POTs system, conversely, at higher values, the sulfite anions trend to display μ , μ_2 , μ_3 or μ_6 modes as inorganic ligands or linkers, instead of structure-directing templates, for example, the vanadium-sulfite POMs^{22a} $(\text{NH}_4)_2(\text{Et}_4\text{N})[(\text{V}^{\text{IV}}\text{O})_6(\mu_4\text{-O})_2(\mu_3\text{-OH})_2(\mu_3\text{-SO}_3)_4(\text{H}_2\text{O})_2]\text{Cl}\cdot\text{H}_2\text{O}$ (prepared at pH 4.5) and *trans* $-(\text{NH}_4)_2[\text{V}^{\text{IV}}(\text{OH})_2(\mu\text{-SO}_3)_2]$ (prepared at pH 6.0), the sulfite anions here display μ or μ_3 modes; the polyoxomolybdenum sulfite complexes^{22b} $(\text{NH}_4)_{20}[(\text{Mo}_2\text{V}^{\text{IV}}\text{O}_4)_6(\mu_2\text{-SO}_3)_12(\mu_3\text{-SO}_3)_4]\cdot4\text{H}_2\text{O}$ (prepared at pH 5.0), $(\text{NH}_4)_{15}\{\text{Na}[(\text{Mo}_2\text{V}^{\text{IV}}\text{O}_4)_6(\mu_2\text{-SO}_3)_3(\mu_6\text{-SO}_3)_2]\}_2\cdot5\text{H}_2\text{O}$ (prepared at pH 5.5), $(\text{NH}_4)_8[(\text{Mo}_2\text{V}^{\text{IV}}\text{O}_4)(\text{SO}_3)_4(\mu_2\text{-SO}_3)]\cdot2\text{H}_2\text{O}$ (prepared at pH 6.0), the sulfite anions here display μ_2 , μ_3 , or μ_6 modes. Thus, we primarily conclude that the powerful sulfite anions reveal different coordination modes at different pH value in POMs, which introduce the necessary diversity into POM systems and allow access to new libraries of building blocks.

Structural Analysis. Single-crystal X-ray diffraction analysis (Table 3) indicates that the polyanion of **1**, $[\text{Ce}_2(\text{H}_2\text{O})_6\text{W}_{22}\text{O}_{72}(\text{OH})_4]^{10-}$, has an interesting “S”-shaped topology similar to the $\{\text{W}_{22}\}$ iso-POT cluster⁶ (Figure 1, Figures S1 and S5 in the Supporting Information). It is constructed from two nine-coordinated Ce^{III} ions and two $\{\text{W}_{11}\}$ units,⁶ two Ce^{III} centers located at the inflection point, which are linked to each other and further coordinate to two lacunary $\{\text{W}_{11}\}$ subunits through two μ_3 -oxo bridges to form

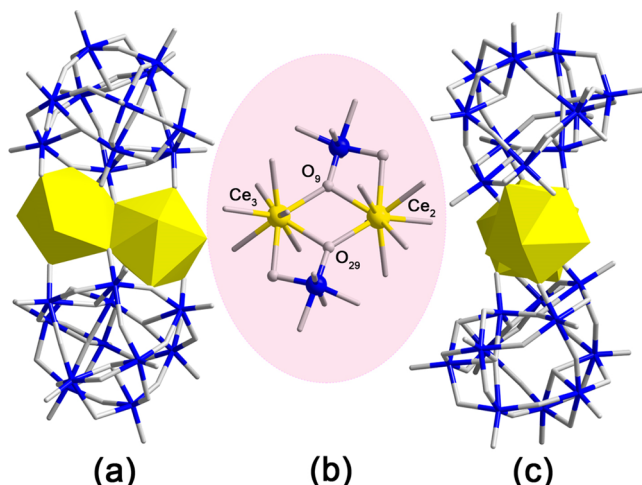


Figure 1. Polyhedral and ball-and-stick representation of polyanion of **1**: (a) top view, (b) connection patterns the two cerium centers, (c) side view. Color code: W (blue); Ce (yellow); and O (gray).

the final dimer structure (bond lengths: $\text{Ce}_3\text{-O}_9$ 2.498, $\text{W}_9\text{-O}_9$ 1.833, $\text{Ce}_2\text{-O}_9$ 2.529, $\text{Ce}_3\text{-O}_{29}$ 2.540, $\text{W}_6\text{-O}_{29}$ 1.797, $\text{Ce}_2\text{-O}_{29}$ 2.537 Å) (Figure 1b). The $\{\text{W}_{11}\}$ subunits (Figure 3a) here remains analogous to the framework of the $[\text{H}_4\text{W}_{11}\text{O}_{38}]^{6-}$ reported in 1988,^{12b} which has already been proved to be an “active” building block in an effort to discover new members of iso-POTs family. The bond-valence sum²³ (BVS) results clearly indicate that each $\{\text{W}_{11}\}$ unit occupied the protonation degree of 2.

X-ray crystallographic analysis of **2** presents that $[\text{Ce}_4(\text{H}_2\text{O})_{12}\text{W}_{44}\text{O}_{144}(\text{OH})_{12}]^{24-}$ is a tetrameric polyanion composed of four novel $\{\text{CeW}_{11}\}$ subunits (Figure 2, Figures

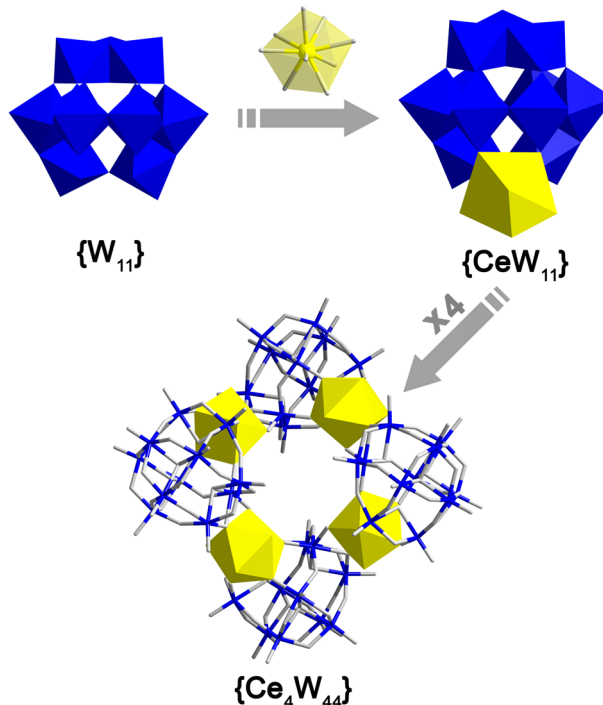


Figure 2. Polyhedral and ball-and-stick representation of polyanion of **2**. Color code: W (blue); Ce (yellow); and O (gray).

S2 and S6 in the Supporting Information). The $\{\text{W}_{11}\}$ unit (Figure 3b) which derivatives from the α -Keggin iso-POTs type $[\text{H}_2\text{W}_{12}\text{O}_{40}]^{6-}$ by losing of one $\{\text{WO}_6\}$ octahedron, is different from that of **1** (Figure 3a), which may be mainly due to the diverse pH values during the reactions. One nine-coordinate Ce^{III} ion is filled in the vacant site of $\{\text{W}_{11}\}$ fragment to form the $\{\text{CeW}_{11}\}$ subunits via four μ_2 -oxo bridges (Figure 3c): $\text{W}_4\text{-O}_{34}\text{-Ce}_1$, $\text{W}_5\text{-O}_{27}\text{-Ce}_1$, $\text{W}_7\text{-O}_{37}\text{-Ce}_1$, and $\text{W}_9\text{-O}_{32}\text{-Ce}_1$ (bond lengths: $\text{W}_4\text{-O}_{34}$ 1.783, $\text{W}_5\text{-O}_{27}$ 1.811, $\text{W}_7\text{-O}_{37}$ 1.738, $\text{W}_9\text{-O}_{32}$ 1.759, $\text{Ce}-\text{O}$ 2.468–2.587 Å). The tetrameric architecture of **2** is constructed from the coordinations of the cerium ion within one $\{\text{CeW}_{11}\}$ subunit and the bridging and terminal oxygen atoms within the other $\{\text{CeW}_{11}\}$ subunit. Moreover, the four separate cerium ions form a “square-planar-like” configuration¹⁰ followed by each one situated at the corners of the square unit (see Figure S2 in the Supporting Information). Each pair of two opposite $\{\text{W}_{11}\}$ units represent a “V”-shaped arrangement, which is cross located above and below the “cerium plane”, respectively, resulting in **2** crystallized in space group $I4_{1/a}$ with a tetragonal structure. Both the related architectures of polyanions of **1** and **2** are unexpected in Ln-containing iso-POTs, which reveal the di- or tetra-

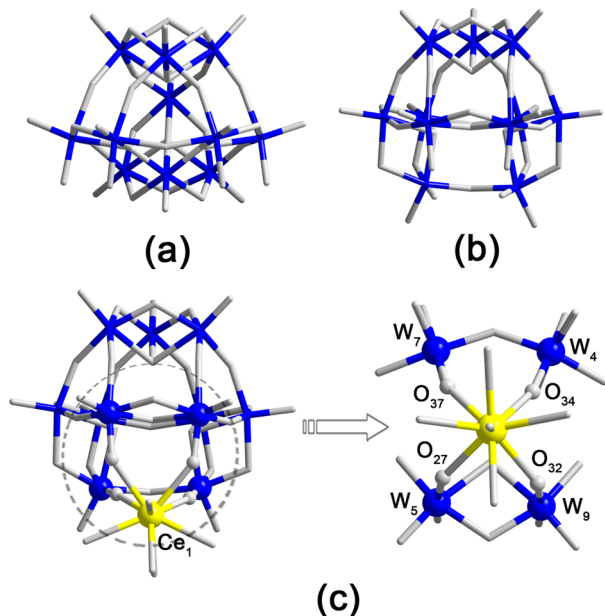


Figure 3. Ball-and-stick representations of two types of $\{W_{11}\}$ units in (a) 1 and (b) 2. Connection patterns of the $\{CeW_{11}\}$ subunits in 2 (c). Color code: W (blue); Ce (yellow); and O (gray).

topologies based upon the linkage of two types of $\{W_{11}\}$ building blocks bridged via the cerium(III) centers. The BVS calculations indicate that each $\{W_{11}\}$ unit appears to be trebly protonated with the protons located at the three μ_4 -oxo bridges. The polyanion of 3 consists of a isopolyanion unit $[H_2W_{28}O_{95}]^{20-}$ that contains two undecatungstate $\{W_{11}\}$ fragments, a hexatungstate fragment $\{W_6\}$ and two $\{Ce(H_2O)_5\}^{3+}$ supporting groups as above-mentioned in polyanion of 1.¹⁶ This polyanion was first reported by Kortz et al. in 2009 isolated as sodium salt in the solid state, but here 3 was isolated by the sodium–organic amine and extra cerium cations.

The polyoxoanion of 4 represents a trimetric Ce^{III}-stabilized POTs nanocluster structure, which was isolated as a mixed sodium–organic amine salt $[C_2H_8N]_2Na_7[\alpha-SW_7O_{28}]\cdot\{Ce_2(H_2O)_6\}(W_3O_6)\{\alpha-SW_9O_{32}\}\{\alpha-SW_9O_{31}(OH)\}\cdot18H_2O$ (Figure 4, Figures S3 and S7 in the Supporting Information). The SO₃²⁻ here acts as a heteroanion template, which has a lone pair of electrons and forms three bonds with oxygen atoms in trigonal configurations, effectively giving rise to “open” lacunary units instead of “closed” Keggin-type clusters. It can also be viewed as a “inorganic ligand”.^{18a} The trimetallic polyanion can be divided into four subunits: one lacunary Keggin-type $\{\alpha-SW_7\}$ unit, two lacunary Keggin-type $\{\alpha-SW_9\}$ units and a $\{Ce_2W_3\}$ core (Figure 4). As shown in Figure 5, the $\{\alpha-SW_7\}$ unit is derived from the trilacunary Keggin-type $\{\alpha-SW_9\}$ unit by losing two $\{WO_6\}$ octahedra from two adjacent $\{W_3O_{13}\}$ units. The SO₃²⁻ anion shows two types of μ_7 -SO₃²⁻ and μ_9 -SO₃²⁻ coordination modes with the bond lengths ranging from 1.508(18) to 1.572(18) Å (Figure 5 and Table S7 in the Supporting Information), which are a little shorter than those of SeO₃²⁻ and TeO₃²⁻ heteroanion templates in cerium(III)-containing POTs.^{10,18} The SO₃²⁻ anion supports the peripheral $\{W_7\}$ unit to exhibit an unusual μ_7 -coordination mode, which is different from the reported μ_7 -SO₃²⁻ in POTs existing in the Dawson-type polyanion, such as $[W_{18}O_{56}(SO_3)_2(H_2O)_2]$ ^{8-7,11} only seven W centers of each $\{SW_9\}$ fragment are connected to the SO₃²⁻ anions. Moreover,

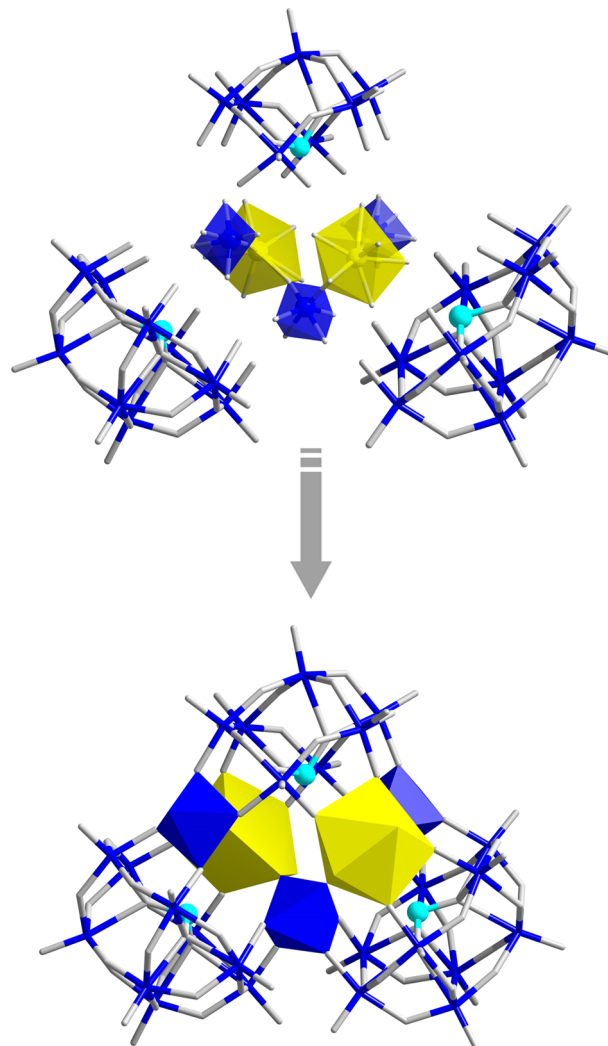


Figure 4. Polyhedral and ball-and-stick representation of the basic building blocks (top) and their connection modes in the polyanion of 4 (bottom). Color code: W (blue); Ce (yellow); S (indigo); and O (gray).

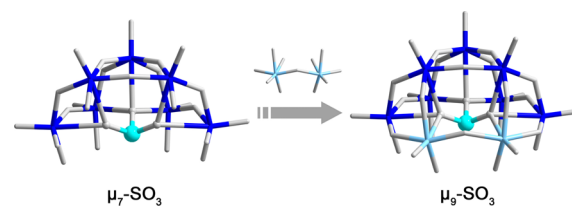


Figure 5. Ball-and-stick representation of $\{\mu_7\text{-SO}_3\}$ and $\{\mu_9\text{-SO}_3\}$ units in the lacunary Keggin-type fragments of 4. Color code: W (blue or light blue); S (indigo); and O (gray).

one of the Keggin-type $\{\alpha-SW_9\}$ units appears to be single protonated with the proton located at one of the three μ_4 -oxo bridges according to the BVS calculations. Furthermore, all the 4f metal cerium(III) centers represent eight-coordinated modes to stabilize three lacunary Keggin-type units, finally resulting in the formation of the polyoxoanion of 4, which is the first Ln-containing POT with sulfur heteroatom to date.^{8a,9b}

The formation of this unprecedented Ce^{III}-stabilized cluster based on the SO₃²⁻ heteroanion templates may be ascribed to four key factors: (1) the SO₃²⁻ acts as a heteroanion template

(due to the lone pair of electrons) with the multiple coordination modes (eg., μ_7 and μ_9), which introduces the necessary diversity into POT clusters and allows an access to the new library of building blocks (eg., Keggin-type $\{\alpha\text{-SW}_7\}$ unit) during the design and synthesis of high-nuclear tungsten sulfite system; (2) the pH of the reaction has been verified to control the formation process, all the five clusters were prepared under the same reaction conditions but with different pH. Such a low and precise pH (pH 2.50) “sensitizes” the sulfite anion to act as structure-directing template for the engineering of this compound; (3) the existence of cerium centers may also be important due to its high coordination number, long bonds, and large radius. Two eight-coordinated Ce^{3+} ions coordinate with three extra $\{\text{WO}_6\}$ octahedra to form the $\{\text{Ce}_2\text{W}_3\}$ core (Figure 4) with the bond lengths ranging from 2.360(18) to 2.80(3) Å (see Table S8 in the Supporting Information), which stabilizes three lacunary Keggin-type units at the same time; (4) the bulky use of protonated organic amine cations is beneficial for the isolation of this cluster.^{11b}

Structural analysis reveals that the polyoxoanion of **5** has a dimeric structure constructed from two identical $\{\text{Ce}_2\text{W}_{36}\}$ subunits related by an inversion center (Figure 6, Figures S4

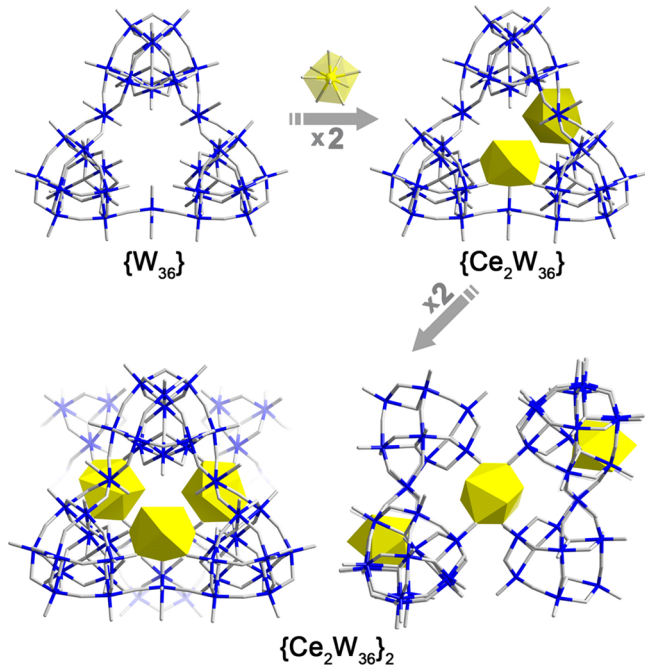


Figure 6. Polyhedral and ball-and-stick representation of polyanion of **5**. Color code: W (blue); Ce (yellow); and O (gray).

and S8 in the Supporting Information). As shown in Figure 6, in each $\{\text{Ce}_2\text{W}_{36}\}$ subunits, one Ce^{3+} ion is trapped at the bottom of the central cavity in $\{\text{W}_{36}\}$ subunit and the other Ce^{3+} ion attaches to the flank of the $\{\text{W}_{36}\}$ subunit. The two $\{\text{W}_{36}\}$ subunits are bridged by two “attached” Ce centers and stabilized by two “trapped” Ce centers. The Ln ions may be the first time to be implanted into the $\{\text{W}_{36}\}$ -based inorganic crown in the host–guest chemistry.^{12f,24} The $\{\text{W}_{36}\}$ iso-POT segment has already been discovered by Cronin et al. in 2004^{12f} and now it is efficiently introduced here as an iso-POT building block, whereas, it is worthy to mention that the coordination mode of W(27) bridge is different from the other two W(10) and W(30) bridges in each $\{\text{W}_{36}\}$ cluster of **5**, which uses only two W–O bonds (W₂₇–O₂₀ 1.917, W₂₇–O₂₂ 1.908 Å) as the

bridges to link the two adjacent $\{\text{W}_{11}\}$ units because the “trapped” Ce centers present a new $\{\text{W}_{36}\}$ iso-POTs segment (Figure 7). The BVS calculations indicate that two oxygen

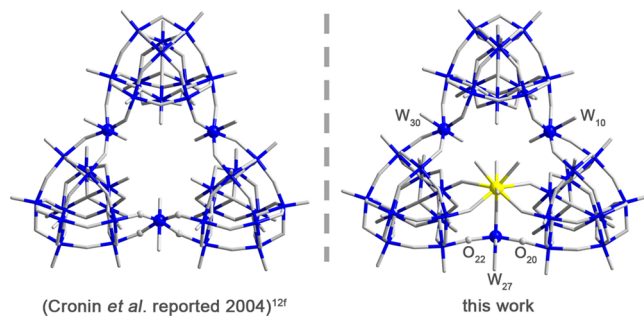


Figure 7. Ball-and-stick representations of two types of $\{\text{W}_{36}\}$ units. Color code: W (blue); Ce (yellow); and O (gray).

atoms in the unusual W(27) bridge are doubly protonated which can be considered as the “guest” cerium metal-induced process just in contrary to the aqua-ligand-induced capability of “trapping” guest metal ions reported by Wang’s group²⁵ (The results of BVS calculations for all the oxygen atoms of **1–5** are listed in Tables S2–S6 in the Supporting Information). In addition, BVS, elemental analysis, EPR spectra, XPS spectra, and DFT calculations indicate that the oxidation states of Ce^{III} centers in **1–5** (see Section 3 in the Supporting Information).

Structural Features. The discovery of **1**, **2**, **3**, and **5** reveals the powerful abilities of iso-POTs ligands coordinating to the Ce centers. Different types of the lacunary $\{\text{W}_{11}\}$ units along with Ce centers achieve variant Ce-bridged dimeric or tetrameric architecture respectively: the “S”-shaped topology $\{\text{Ce}_2\text{W}_{22}\}$ and the novel $\{\text{Ce}_4\text{W}_{44}\}$ containing α -Keggin-type $\{\text{W}_{11}\}$ units. In addition, bigger ligands, namely the “V”-shaped $\{\text{W}_{28}\}$ and triangular-shaped $\{\text{W}_{36}\}$ units, trend to be stabilized by the Ce centers to form $\{\text{Ce}_2\text{W}_{28}\}$ and $\{\text{Ce}_2\text{W}_{36}\}_2$. Different sizes of iso-POTs ligands may guide bridging or stabilizing functions of high coordinated Ce centers. As for **4**, it is the first Ln-containing POTs with sulfur heteroatom, involving two types of lacunary Keggin-type $\{\alpha\text{-SW}_7\}$ and $\{\alpha\text{-SW}_9\}$ ligands with μ_7 and μ_9 -coordination modes. The diverse coordination modes for the sulfite anion show the important roles of the design and synthesis of novel sulfite-based Ln-containing materials.

Electrospray Ionization Mass Spectroscopy (ESI-MS) Studies. ESI-MS studies²⁶ of **1**, **2**, **3**, and **4** dissolved in water confirmed that the four compounds retained its integrity in solution through all the m/z values of the main peaks, which can be assigned to their different charge/cation states. For polyoxoanion of **1**, the strong peaks centered at m/z 1150.3 and 1438.1 correspond to the charges of -5 and -4 , respectively. The other peak, which has an m/z value of 1942.8 and lower intensity compared to the other two, has a charge of -3 (see Figure S10 in the Supporting Information). **2** shows only one peak at m/z 2350.3 with the charge of -5 and retains its structural integrity (see Figure S11 in the Supporting Information). Accordingly, we found the two clusters associated with $[\text{C}_2\text{H}_8\text{N}]^+$, Na^+ , and H^+ ions dominated the solution of redissolved pure **1** or **2**. As for the polyoxoanion of **3**, the peaks centered at m/z 2066.3 and 2758.1 correspond to the charges of -4 and -3 , respectively (see Figure S12 in the Supporting Information). The observed peaks of **4** were assigned to $\{\text{NaH}_3[\text{Ce}_2(\text{H}_2\text{O})_6\text{S}_3\text{W}_{28}\text{O}_{97}(\text{OH})]\}^{5-}$, $\{(\text{C}_2\text{H}_8\text{N})-$

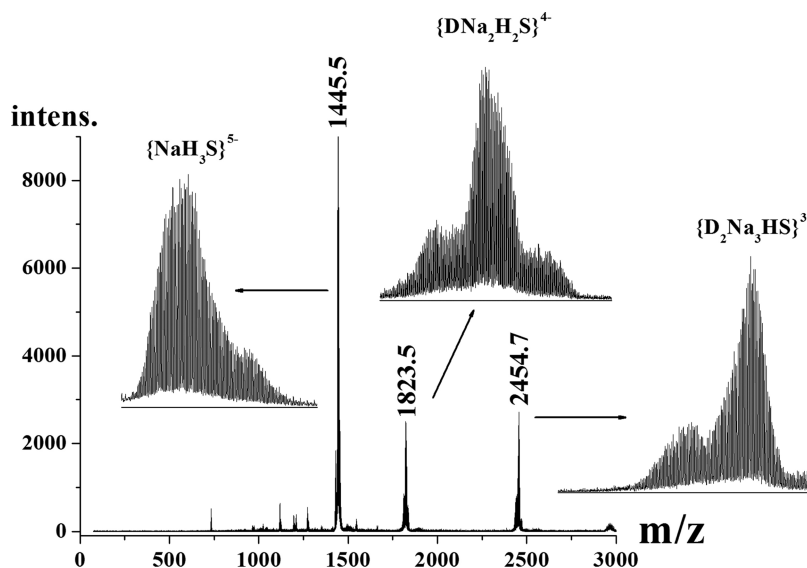


Figure 8. ESI-MS of **4** in H_2O .

$\text{Na}_2\text{H}_2[\text{Ce}_2(\text{H}_2\text{O})_6\text{S}_3\text{W}_{28}\text{O}_{97}(\text{OH})]^{4-}$, and $\{(\text{C}_2\text{H}_8\text{N})_2\text{Na}_3\text{H}[\text{Ce}_2(\text{H}_2\text{O})_6\text{S}_3\text{W}_{28}\text{O}_{97}(\text{OH})]\}^{3-}$, giving envelopes centered at m/z 1445.5, 1823.5, and 2454.7, respectively (Figure 8). In the case of **5**, the main fragment (e.g., $\{\text{Ce}_2\text{W}_{36}\}$) has been observed associated with $[\text{C}_2\text{H}_8\text{N}]^+$, Na^+ , and H^+ ions (see Figure S13 in the Supporting Information). The assignments of peaks of the five polyoxoanions are listed in Tables S14–S18 in the Supporting Information.

X-ray Photoelectron Spectroscopy (XPS). The XPS investigations on **1**, **2**, **4**, and **5** were performed to confirm the valence states of W, Ce and S. The XPS spectra of Ce centers: the peaks around 904.0 and 885.5 eV in the energy regions of $\text{Ce} 3d_{3/2}$ and $\text{Ce} 3d_{5/2}$ correspond to Ce^{3+} (Figure S14a for **1**, S14b for **2**, S14c for **4**, and S14d for **5** in the Supporting Information).^{27a} The XPS spectra of W centers: the peaks around 37.2 and 35.1 eV in the energy regions of $\text{W} 4f_{5/2}$ and $\text{W} 4f_{7/2}$ are confirmed to be W^{6+} centers represented in Figure S15 in the Supporting Information.^{27b} Moreover, Figure S14e in the Supporting Information shows the existence of sulfite in **4** with the S 2p peak located at 167.8 eV,^{27c,d} further confirming the combination of Ce^{3+} ions and SO_3^{2-} heteroanion templates to lead to the formation of **4**. In addition, low contents for the Ce and S compared to W in these compounds cause the noisy XPS spectra for Ce and S if compared them to those for the tungsten atoms.²⁸ Besides, the Ce 3d XPS spectra of Ce-containing compounds are known to be complicated due to the hybridization of the Ce 4f with ligand orbitals and fractional occupancy of the 4f valence orbitals.^{28f,g}

Electrochemistry. Cyclic voltammetry (CV) experiments were performed to examine the redox properties of **1–5** in 0.5 M $\text{H}_2\text{SO}_4/\text{Na}_2\text{SO}_4$ solution. All of the compounds show the waves associated with the reduction of W^{VI} centers between -1.143 and -0.333 V as well as the redox process of Ce^{III} centers from $+0.673$ to $+0.867$ V (vs Ag/AgCl), which are in good agreement with reported Ce^{III} -containing POT compounds.^{8c,10,14,29}

In a sulfate pH 5.0 medium, the CV of **1** (Figure 9) (5×10^{-4} M) at a scan rate of 30 mV s^{-1} shows two separated quasi-reversible redox couples of waves at $E_{1/2} = -1.102$ V (I/I') and $E_{1/2} = -0.605$ V (II/II') [$E_{1/2} = (E_{\text{pa}} + E_{\text{pc}})/2$] (vs Ag/AgCl),

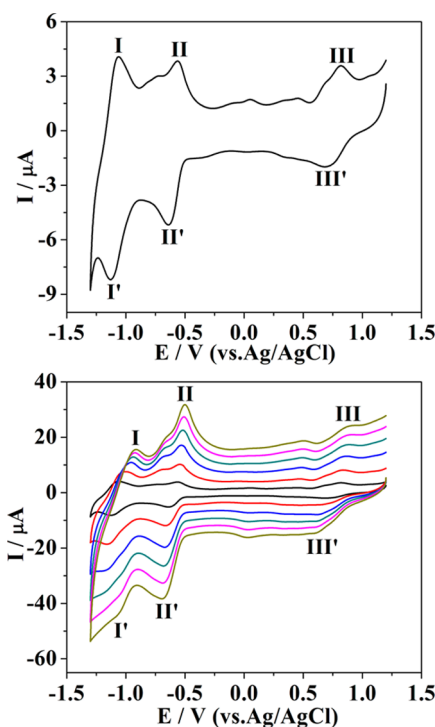


Figure 9. Cyclic voltammograms of **1** in 0.5 M $\text{H}_2\text{SO}_4/\text{Na}_2\text{SO}_4$ solution (pH 5.0). POM concentrations = 5×10^{-4} M. The scan rate was 30 mV s^{-1} (top). Cyclic voltammograms at different scan rates: from inside to out: 30, 100, 200, 300, 400, and 500 mV s^{-1} (bottom). The working electrode was glassy carbon, and the reference electrode was Ag/AgCl.

corresponding to the redox processes of W^{VI} centers, respectively (Table 4). When taken at a higher concentration (10^{-3} M) (Figure 10), one more quasi-reversible couple at $E_{1/2} = -0.778$ V (vs Ag/AgCl) (Table 4) between the aforementioned two couples was observed. This additional couple is hard to be recognized at a low concentration (5×10^{-4} M), and retains weaker at a high concentration (10^{-3} M). Also, Figure 11 compares the CVs of **1** and the $[\text{H}_4\text{W}_{11}\text{O}_{38}]^{6-}$ building block^{12b} recorded in 0.5 M $\text{H}_2\text{SO}_4/\text{Na}_2\text{SO}_4$ solution

Table 4. Redox Peak Potentials for all the Tungsten Waves Determined by Cyclic Voltammetry in 0.5 M H₂SO₄/Na₂SO₄ Solution (pH 5.0) for W₁₁ and 1^a

	E _{pa} (V)	E _{pc} (V)	E _{1/2} (V)	ΔE _p (mV)
Ce ₂ W ₂₂ ^a (pH 5.0)	-0.565	-0.644	-0.605	79
	-1.061	-1.143	-1.102	82
Ce ₂ W ₂₂ ^b (pH 5.0)	-0.522	-0.600	-0.561	78
	-0.751	-0.805	-0.778	54
W ₁₁ ^c (pH 5.0)	-1.010	-1.113	-1.062	103
	-0.339	-0.428	-0.384	89
	-0.579	-0.632	-0.606	53
1 (pH 5.0)	-0.956	-1.012	-0.984	56

^aPOM concentrations = ^a5 × 10⁻⁴ M. ^b10⁻³ M. ^c2 × 10⁻³ M.

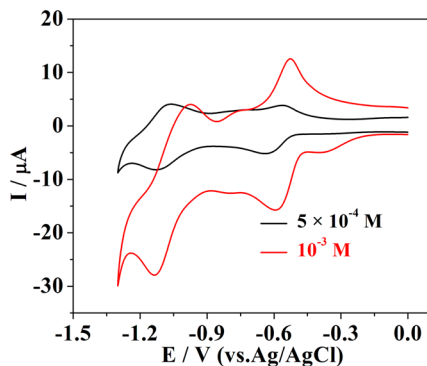


Figure 10. Cyclic voltammograms of 1 in 0.5 M H₂SO₄/Na₂SO₄ solution (pH 5.0) in different concentrations. The scan rate was 30 mV s⁻¹. The working electrode was glassy carbon, and the reference electrode was Ag/AgCl.

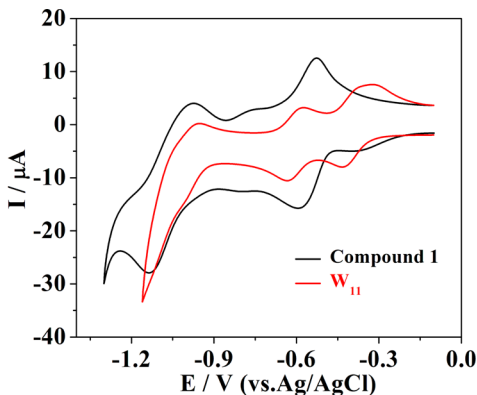


Figure 11. Cyclic voltammograms of 1 (black) and W₁₁ (red) in 0.5 M H₂SO₄/Na₂SO₄ solution (pH 5.0). POM concentrations = 10⁻³ M (1) and 2 × 10⁻³ M (W₁₁). The scan rate was 30 mV s⁻¹. The working electrode was glassy carbon, and the reference electrode was Ag/AgCl.

(pH 5.0, scan rate was 30 mV s⁻¹). This study might allow us to extract some distinct features of 1 which is due to the two bridged Ce centers. The CV of [H₄W₁₁O₃₈]⁶⁻ is characterized by three redox steps located at -0.384, -0.606, and -0.984 V (vs Ag/AgCl) (Table 4). Compared to 1, there is a potential shift of 177, 172, and 78 mV toward the positive region for the first, second, and third redox steps, respectively (Table 4). These differences observed here may be due to the extra Ce centers and different negative charges of them under such conditions.^{30a} The exact positions and strength of the W-waves evolve upon increasing the pH of the supporting electrolyte³¹

(see Figure S16 in the Supporting Information). As expected, the CV pattern of W-waves moves toward negative potentials when the pH increases^{31a,c} (see Table S19 in the Supporting Information), in addition, the second redox couple is gradually clear and the other two couples fade but still easy to be identified when the pH is sequentially increased from 5.0 to 6.0. This observation accords with the previous reports because W-waves are usually more likely to split with the increase of the electrolyte pH.^{30,31} In the positive region of potentials, we observed an oxidation peak located at E_{pa} = 0.828 V (vs Ag/AgCl), whereas the ΔE_p value of 109 mV for the oxidation process of interest suggests a quasi-reversible one-electron process (the theoretical value of ΔE_p for a reversible electron transfer is about 59 mV),^{29a} which is attributed to the cerium(IV/III) redox processes (Table 6). After increasing the scan rates, from 30 to 500 mV s⁻¹ (Figure 9), the first W-based redox couple gradually enhance while the second couple shows a weaken trend, and the peak positions remain no shifts as described in the literature for other POMs.³¹ Above 100 mV s⁻¹ the peak currents were proportional to the square root of the scan rate, demonstrating that the redox process becomes diffusion-controlled, similar behaviors were observed in the case of the other compounds (see Figure S17 in the Supporting Information).

As for 2 (Figure 12a) at a scan rate of 30 mV s⁻¹, an unforgettable and sharp peak potential with a large current

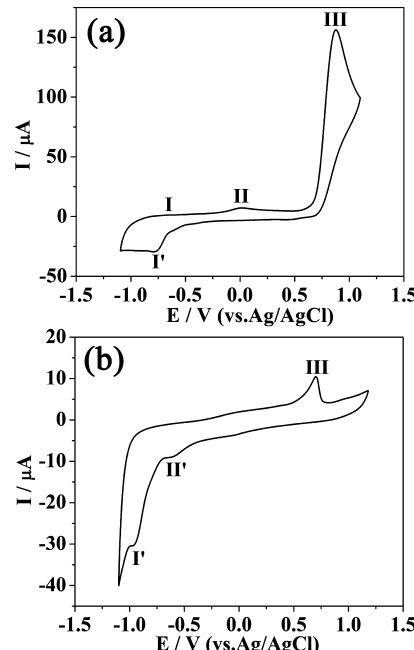


Figure 12. Cyclic voltammograms of 2 (a) and 3 (b) in 0.5 M H₂SO₄/Na₂SO₄ solution (pH 4.5 for 2, pH 3.5 for 3). POM concentrations = 5 × 10⁻⁴ M. The scan rate was 30 mV s⁻¹. The working electrode was glassy carbon, and the reference electrode was Ag/AgCl.

intensity appeared at +0.867 V (III) confirms that the irreversible cerium(IV/III) process (Table 6). 1 and 2 possess two types of {W₁₁} units that achieve different coordination environment of W centers thus the W-waves in the negative region varied: one single oxidation wave is observed at E_{pa} = -0.015 V (II) (see Table S20 in the Supporting Information) and it gradually begins to be found obviously after increasing the scan rates (see Figure S18 in the Supporting Information);

the other remains a quasi-reversible redox couple with the corresponding $E_{1/2}$ peak potentials located at -0.723 V (I/I') (see Table S20 in the Supporting Information). Similar W-waves were also found in 3 (Figure 12b). The negative region of potential values represents two obvious reduction waves appeared at -0.613 (II') and -0.965 V (I'), which were also assigned to W^{VI} centers respectively (Table S20 in the Supporting Information). As the large current intensity Ce^{III} wave in 2, we also found one wave near at $E_{pa} = +0.726$ V (III) (vs Ag/AgCl) (Figure 12b), indicating the irreversible cerium(IV/III) process (Table 6).

In the case of 4, the unique sulfur-containing POT cluster, one oxidation wave was observed on positive potential located at $+0.232$ (III) (Figure 13) thus confirming the irreversible

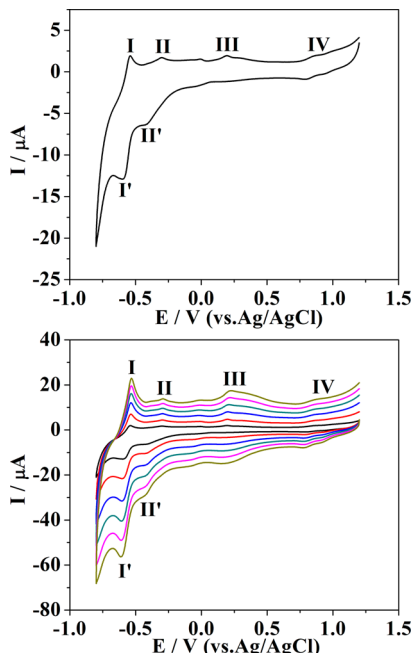


Figure 13. Cyclic voltammograms of **4** in 0.5 M $\text{H}_2\text{SO}_4/\text{Na}_2\text{SO}_4$ solution (pH 2.5). POM concentrations $= 5 \times 10^{-4}$ M. The scan rate was 30 mV s^{-1} (top). Cyclic voltammograms at different scan rates: from inside to out: $30, 100, 200, 300, 400$, and 500 mV s^{-1} (bottom). The working electrode was glassy carbon, and the reference electrode was Ag/AgCl.

oxidation of S^{IV} centers according to the previous reports.^{11b} Another oxidation peak at $E_{pa} = +0.863$ V (IV) (vs Ag/AgCl) was attributed to the irreversible cerium(IV/III) process just as the peaks in 2 and 3. The negative region of potential values represents two well-separated quasi-reversible redox couples of waves at $E_{1/2} = -0.589$ V (I/I') and $E_{1/2} = -0.355$ V (II/II') (vs Ag/AgCl), corresponding to the redox processes of W^{VI} centers, respectively. In aqueous solution, the redox behavior of **4** is pH dependent, as seen in Figure 14. As the pH of the electrolyte increases from 2.5 to 4.5, the second redox waves are shifted in the direction of negative potentials and the current intensity decrease gradually. This is a well-known electrochemical behavior for the majority of the POMs about the W-waves.^{29–31} Table 5 summarizes redox peak potential values for the second waves of **4** in 0.5 M $\text{H}_2\text{SO}_4/\text{Na}_2\text{SO}_4$ solution at pH 2.5, 3.5, and 4.5. Furthermore, no shifts or shapes of the irreversible cerium(IV/III) process changed because of no H⁺ or OH⁻ involved during this process (Figure 14).

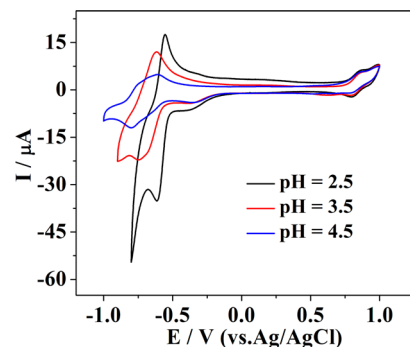


Figure 14. Cyclic voltammograms of **4** at different pH values: pH 2.5 (black), pH 3.5 (red), pH 4.5 (blue) in 0.5 M $\text{H}_2\text{SO}_4/\text{Na}_2\text{SO}_4$ solution. POM concentrations $= 5 \times 10^{-4}$ M. The scan rate was 30 mV s^{-1} . The working electrode was glassy carbon, and the reference electrode was Ag/AgCl.

Table 5. Redox Peak Potentials for the Second Tungsten Waves Determined by Cyclic Voltammetry in 0.5 M $\text{H}_2\text{SO}_4/\text{Na}_2\text{SO}_4$ Solution at pH 2.5, 3.5, and 4.5 for **4**

pH	E_{pa} (V)	E_{pc} (V)	$E_{1/2}$ (V)	ΔE_p (mV)
2.5	-0.560	-0.617	-0.589	57
3.5	-0.630	-0.703	-0.667	73
4.5	-0.731	-0.803	-0.767	72

Figure 15 shows the main characteristic peaks associated with W centered redox couples of **5** in the region -1.000 to $+1.200$ V of potential values versus Ag/AgCl at a scan rate of 30 mV s^{-1} . Scanning toward the negative region of potential values, the reduction of W centers occurs through three quasi-reversible (vs Ag/AgCl) redox couples, with the corresponding $E_{1/2}$ peak

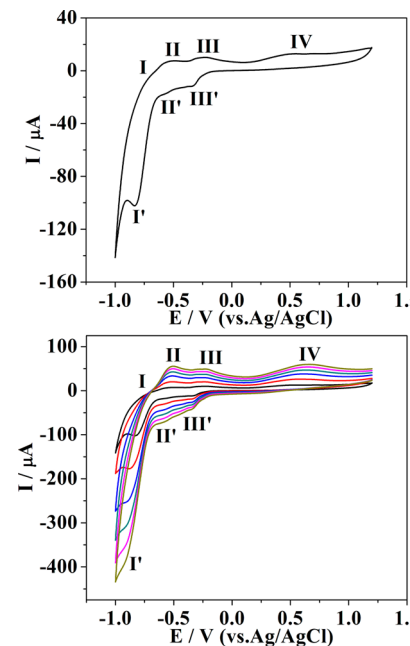


Figure 15. Cyclic voltammograms of **5** in 0.5 M $\text{H}_2\text{SO}_4/\text{Na}_2\text{SO}_4$ solution (pH 1.5). POM concentrations $= 5 \times 10^{-4}$ M. The scan rate was 30 mV s^{-1} (top). Cyclic voltammograms at different scan rates: from inside to out: $30, 100, 200, 300, 400$, and 500 mV s^{-1} (bottom). The working electrode was glassy carbon, and the reference electrode was Ag/AgCl.

potentials located at -0.297 (III/III'), -0.546 (II/II'), and -0.786 V (I/I') (see Table S21 in the Supporting Information), respectively. Compared to the $\{W_{36}\}^{12f}$ reduction peaks (see Figure S19 in the Supporting Information), there is a potential shift of 166, 102, and 71 mV for the first, second, and third reduction steps, respectively, each in favor of W_{36} reduction (see Table S21 in the Supporting Information). These differences may be due to the influence of the coordinate Ce centers, the oxidation peak of it is located at $E_{pa} = +0.673$ V (IV) (vs Ag/AgCl) in the positive region (Table 6).

Table 6. Oxidation Peak Potentials, E_{pa} , for the Ce^{III} Waves Determined by Cyclic Voltammetry in 0.5 M H₂SO₄/Na₂SO₄ Solution for 1, 2, 3, and 5

E_{pa} (V)	compounds			
	Ce ₂ W ₂₂	Ce ₄ W ₄₄	Ce ₂ W ₂₈	{Ce ₂ W ₃₆ }
0.828	0.867	0.726	0.673	

As for **1**, **2**, **3**, and **5**, they are all Ce^{III}-containing iso-POTs. The iso-POTs ligands, involving two types of the lacunary $\{W_{11}\}$ units, the "V"-shaped $\{W_{28}\}$ unit that contains two $\{W_{11}\}$ units, and the triangular-shaped $\{W_{36}\}$ unit that contains three $\{W_{11}\}$ units, were stabilized or bridged by the Ce^{III} centers. Table 6 summarizes Ce^{III}-waves for the four compounds. It is possible and easy to see that similar Ce^{III} oxidation peak potentials for **1** ($E_{pa} = +0.828$ V) and **2** ($E_{pa} = +0.867$ V) (vs Ag/AgCl) were observed in view of their similar $\{W_{11}\}$ ligands, whereas, **1** shows one redox wave ($E_{1/2} = +0.774$ V (vs Ag/AgCl)), whereas **2** exhibits one oxidation peak, which may mainly be due to the fact that the different types of $\{W_{11}\}$ units vary the coordination environment of Ce^{III} centers: two Ce^{III} ions are linked to each other and further coordinate to two lacunary $[H_4W_{11}O_{38}]^{6-}$ units, achieving the ditopology in **1**, whereas, one Ce^{III} ion is filled in the vacant site of $[H_3W_{11}O_{39}]^{9-}$ units to yield the $\{CeW_{11}\}$ subunits thus forming the tetra-topology in **2**. **3** also reveals one oxidation peak potential at $E_{pa} = +0.726$ V (vs Ag/AgCl) as well as that in **2**, but there is a potential shift of 141 mV toward to the negative region. Thus, we can see Ce^{III} oxidation potential correlates the size of coordinated iso-POT ligands. For the small size of $\{W_{11}\}$ units, **1** and **2** possess similar Ce^{III} oxidation peak potentials. As for the larger "V"-shaped $\{W_{28}\}$ unit, **3** possesses Ce^{III} oxidation peak potential at $+0.726$ V (vs Ag/AgCl) toward to the negative region compared to **1** and **2**. More trend to the negative region was observed in **5** ($E_{pa} = +0.673$ V (vs Ag/AgCl)) that contains the largest triangular-shaped $\{W_{36}\}$ unit.

CONCLUSIONS

A versatile one-pot strategy was used to prepare five cerium(III)-containing POTs via pH-controlled (from pH 1.5 to 5.0) and sulfite anion-directed assembly process, which have proved to be the key factors for the successful synthesis of **1–5**. The iso-POTs units, involving two types of the lacunary $\{W_{11}\}$ units, the "V"-shaped $\{W_{28}\}$ unit, and the triangular-shaped $\{W_{36}\}$ unit, were stabilized or bridged by the cerium(III) centers to form **1**, **2**, **3**, and **5**. The isolation of polyanion of **4** at pH = 2.5 is dependent on the combination of cerium(III) centers and SO₃²⁻ heteroanion template, it is the first Ln-containing POTs with sulfur heteroatom. These compounds were characterized by single-crystal X-ray structure analysis, IR

spectroscopy, TG analysis, XPS, and ESI-MS. Moreover, the electrochemical studies in aqueous media showed the redox process of Ce^{III} centers from +0.673 to +0.867 V, the oxidation of the S^{IV} metal center at +0.232 V, and the reduction of W^{VI} centers between -1.143 and -0.333 V, respectively.

In the field of iso-, or hetero-POT-based high-nuclearity clusters, this work may be an important leap: (1) the discovery of polyanions of **1**, **2**, and **5** enriches the family of Ce^{III}-containing iso-POTs clusters with the utilization of iso-POT basic building blocks (eg, $\{W_{11}\}$ and $\{W_{36}\}$); (2) the successful synthesis of **4** may be an important breakthrough, which opens up a novel perspective for the design of sulfur-based POTs functional materials and devices; (3) there is also some key experience during the synthesis, such as pH, the sulfite anion templates, and so on. It is worth noting that the role of the sulfite anion in the formation of these clusters may direct the synthesis of different iso-POTs and promote the use of the building-block principle. Whence, our future work will concentrate on investigating the assembly and the functionality of these clusters with different heteroanion templates (eg., SO₃²⁻, SeO₃²⁻, or TeO₃²⁻).

ASSOCIATED CONTENT

S Supporting Information

Details of additional structural figures, the table of the detailed survey of Ln-containing hetero-POTs, the table of the BVS calculation result of all the oxygen atoms, the Determination of the Ce(III) oxidation state, the IR, TGA, XRD, XPS, ESI-MS characterizations, and electrochemistry, the tables of the assignment of peaks of ESI-MS. This material is available free of charge via the Internet at <http://pubs.acs.org>.

AUTHOR INFORMATION

Corresponding Authors

*E-mail: zmsu@nenu.edu.cn.

*E-mail: wangxl824@nenu.edu.cn

Notes

The authors declare no competing financial interest.

ACKNOWLEDGMENTS

We gratefully acknowledge the financial support from the NNSF of China (21001022, 21171033, 21131001), the NGFR 973 Program of China (2010CB635114), NCET in Chinese University (NCET-10-0282), PhD Station Foundation of Ministry of Education (20100043110003), the FANEDD of the P. R. China (201022), the STDP of Jilin Province (201001169, 20111803), and the FRFCU (09ZDQD003, 10CXTD001).

REFERENCES

- (a) Pope, M. T. *Heteropoly and Isopoly Oxometalates*; Springer, Berlin, 1983. (b) Müller, A.; Peters, F.; Pope, M. T.; Gatteschi, D. *Chem. Rev.* **1998**, *98* (1), 239. (c) Miras, H. N.; Yan, J.; Long, D.-L.; Cronin, L. *Chem. Soc. Rev.* **2012**, *41*, 7403.
- (a) Izarova, N. V.; Pope, M. T.; Kortz, U. *Angew. Chem., Int. Ed.* **2012**, *51*, 9492. (b) Long, D. L.; Tsunashima, R.; Cronin, L. *Angew. Chem., Int. Ed.* **2010**, *49*, 1736. (c) Yamase, T. *Chem. Rev.* **1998**, *98*, 307. (d) Kortz, U.; Müller, A.; van Slageren, J.; Schnack, J.; Dalal, N. S.; Dressel, M. *Coord. Chem. Rev.* **2009**, *293* (19–20), 2315.
- (a) Richmond, C. J.; Miras, H. N.; de La Oliva, A. R.; Zang, H.-Y.; Sans, V.; Paramonov, L.; Makatsoris, C.; Inglis, R.; Brechin, E. K.; Long, D.-L.; Cronin, L. *Nat. Chem.* **2012**, *4*, 1037. (b) de La Oliva, A.

- R.; Sans, V.; Miras, H. N.; Yan, J.; Zang, H.-Y.; Richmond, C. J.; Long, D.-L.; Cronin, L. *Angew. Chem., Int. Ed.* **2012**, *51*, 12759.
- (4) (a) Pradeep, C. P.; Long, D.-L.; Streb, C.; Cronin, L. *J. Am. Chem. Soc.* **2008**, *130*, 14946. (b) Reinoso, S.; Bassil, B. S.; Barsukova, M.; Kortz, U. *Eur. J. Inorg. Chem.* **2010**, 2537. (c) Jiao, Y.-Q.; Qin, C.; Wang, X.-L.; Wang, C.-G.; Sun, C.-Y.; Wang, H.-N.; Shao, K.-Z.; Su, Z.-M. *Chem.—Asian J.* **2014**, *9*, 470–478.
- (5) Fang, X.-K.; Kögerler, P. *Angew. Chem., Int. Ed.* **2008**, *47*, 8123.
- (6) Miras, H. N.; Yan, J.; Long, D.-L.; Cronin, L. *Angew. Chem., Int. Ed.* **2008**, *47*, 8420.
- (7) Miras, H. N.; Chilas, G. I.; Cronin, L.; Kabanos, T. A. *Eur. J. Inorg. Chem.* **2012**, 1620.
- (8) (a) Bassil, B. S.; Kortz, U. *Z. Anorg. Allg. Chem.* **2010**, *636*, 2222. (b) Ritchie, C.; Speldrich, M.; Gable, R. W.; Sorace, L.; Kögerler, P.; Boskovic, C. *Inorg. Chem.* **2011**, *50*, 7004. (c) Chen, W.-L.; Li, Y.-G.; Wang, Y.-H.; Wang, E.-B.; Su, Z.-M. *J. Chem. Soc., Dalton Trans.* **2007**, *41*, 4293. (d) Huang, W.; Francesconi, L. C.; Plenova, T. *Inorg. Chem.* **2007**, *43*, 7861.
- (9) (a) Wassermann, K.; Dickman, M. H.; Pope, M. T. *Angew. Chem., Int. Ed.* **1997**, *36*, 1445. (b) Bassil, B. S.; Dickman, M. H.; Römer, I.; von der Kammer, B.; Kortz, U. *Angew. Chem., Int. Ed.* **2007**, *46*, 6192. (c) Hussain, F.; Conrad, F.; Patzke, G. R. *Angew. Chem., Int. Ed.* **2009**, *48*, 9088. (d) Reinoso, S.; Giménez-Marqués, M.; Galán-Mascarós, J. R.; Vitoria, P.; Gutiérrez-Zorrilla, J. M. *Angew. Chem., Int. Ed.* **2010**, *49*, 8384. (e) Ismail, A. H.; Bassil, B. S.; Yassin, G. H.; Keita, B.; Kortz, U. *Chem.—Eur. J.* **2012**, *18*, 6163. (f) Zhang, Z.-M.; Li, Y.-G.; Yao, S.; Wang, E.-B. *Dalton Trans.* **2011**, *40*, 6475. (g) Cui, K.-Y.; Li, F.-Y.; Xu, L.; Xu, B.-B.; Jiang, N.; Wang, Y.-C.; Zhang, J. *Dalton Trans.* **2012**, *41*, 4871. (h) Yamase, T.; Naruke, H.; Sasaki, Y. *J. Chem. Soc., Dalton Trans.* **1990**, 1687.
- (10) Chen, W.-C.; Li, H.-L.; Wang, X.-L.; Shao, K.-Z.; Su, Z.-M.; Wang, E.-B. *Chem.—Eur. J.* **2013**, *19*, 11007.
- (11) (a) Long, D.-L.; Abbas, H.; Kögerler, P.; Cronin, L. *Angew. Chem., Int. Ed.* **2005**, *44* (22), 3415. (b) Yan, J.; Long, D.-L.; Miras, H. N.; Cronin, L. *Inorg. Chem.* **2010**, *49*, 1819.
- (12) (a) Fuchs, J.; Palm, R.; Hartl, H. *Angew. Chem., Int. Ed. Engl.* **1996**, *35*, 2651. (b) Lehmann, T.; Fuchs, J. Z. *Z. Naturforsch. B* **1988**, *43*, 89. (c) Singer, R.; Gross, H. *Helv. Chim. Acta* **1934**, *17*, 1076. (d) Allmann, R. *Acta Crystallogr. Sect. B* **1971**, *27*, 1393. (e) Chrissafidou, A.; Fuchs, J.; Hartl, H.; Palm, R. Z. *Naturforsch. B* **1995**, *50*, 217. (f) Long, D.-L.; Abbas, H.; Kögerler, P.; Cronin, L. J. *Am. Chem. Soc.* **2004**, *126*, 13880.
- (13) Peacock, R. D.; Weakley, T. J. R. *J. Chem. Soc. A* **1971**, 1836.
- (14) Li, T.-H.; Li, F.; Lü, J.; Guo, Z.-G.; Gao, S.-Y.; Cao, R. *Inorg. Chem.* **2008**, *47*, 5612.
- (15) Ismail, A. H.; Dickman, M. H.; Kortz, U. *Inorg. Chem.* **2009**, *48*, 1559.
- (16) Ismail, A. H.; Bassil, B. S.; Suchoparand, A.; Kortz, U. *Eur. J. Inorg. Chem.* **2009**, 5247.
- (17) Song, L.-Y.; Zhang, D.-D.; Ma, P.-T.; Liang, Z.-J.; Wang, J.-P.; Niu, J.-Y. *CrystEngComm.* **2013**, *15*, 4597.
- (18) (a) Hutin, M.; Long, D.-L.; Cronin, L. *Isr. J. Chem.* **2011**, *51*, 205. (b) Yan, J.; Long, D.-L.; Cronin, L. *Angew. Chem., Int. Ed.* **2010**, *49*, 4117. (c) Gao, J.; Yan, J.; Mitchell, S. G.; Miras, H. N.; Boulay, A. G.; Long, D.-L.; Cronin, L. *Chem. Sci.* **2011**, *2*, 1502. (d) Gao, J.; Yan, J.; Beeg, S.; Long, D.-L.; Cronin, L. *Angew. Chem., Int. Ed.* **2012**, *51*, 3373. (e) Yan, J.; Gao, J.; Long, D.-L.; Miras, H. N.; Cronin, L. J. *Am. Chem. Soc.* **2010**, *132*, 11410. (f) Gao, J.; Yan, J.; Beeg, S.; Long, D.-L.; Cronin, L. J. *Am. Chem. Soc.* **2013**, *135*, 1796.
- (19) (a) Sheldrick, G. SADABS, version 2.10; University of Gottingen: Göttingen, Germany, 2003. (b) Sheldrick, G. M. SHELXL-97, Program for the Refinement of Crystal Structure; University of Gottingen: Göttingen, Germany, 1993. (c) Spek, A. L. PLATON, A Multipurpose Crystallographic Tool; Utrecht University: Utrecht, The Netherlands, 2003.
- (20) (a) Fang, X.-K.; Hansen, L.; Haso, F.; Yin, P.-C.; Pandey, A.; Engelhardt, L.; Slowing, I.; Li, T.; Liu, T.-B.; Luban, M.; Johnston, D. C. *Angew. Chem., Int. Ed.* **2013**, *52*, 10500–10504.
- (21) (a) Long, D.-L.; Kögerler, P.; Cronin, L. *Angew. Chem., Int. Ed.* **2004**, *43*, 1817–1820. (b) Miras, H. N.; Stone, D. J.; McInnes, E. J. L.; Raptis, R. G.; Baran, P.; Chilas, G. I.; Sigalas, M. P.; Kabanos, T. A.; Cronin, L. *Chem. Commun.* **2008**, 4703–4705. (c) Miras, H. N.; Ochoa, M. N. C.; Long, D.-L.; Cronin, L. *Chem. Commun.* **2010**, 8148–8150.
- (22) (a) Miras, H. N.; Raptis, R. G.; Lalioti, N.; Sigalas, M. P.; Baran, P.; Kabanos, T. A. *Chem.—Eur. J.* **2005**, *11*, 2295–2306. (b) Manos, M. J.; Woollins, J. D.; Slawin, A. M. Z.; Kabanos, T. A. *Angew. Chem., Int. Ed.* **2002**, *41*, 2801–2805.
- (23) (a) Brown, I. D.; Altermatt, D. *Acta Crystallogr., Sect. B* **1985**, *41*, 244. (b) Trzesowska, A.; Kruszynski, R.; Bartczak, T. J. *Acta Crystallogr., Sect. B* **2006**, *62*, 745.
- (24) (a) Long, D.-L.; Brücher, O.; Streb, C.; Cronin, L. *Dalton Trans.* **2006**, 2852. (b) McGlone, T.; Streb, C.; Long, D.-L.; Cronin, L. *Chem.—Asian J.* **2009**, *4*, 1612.
- (25) Zhang, Z.-M.; Yao, S.; Li, Y.-G.; Wang, Y.-H.; Qi, Y.-F.; Wang, E.-B. *Chem. Commun.* **2008**, 1650.
- (26) (a) Bosing, M.; Noh, A.; Loose, I.; Krebs, B. *J. Am. Chem. Soc.* **1998**, *120*, 7252. (b) Long, D.-L.; Streb, C.; Song, Y.-F.; Mitchell, S.; Cronin, L. *J. Am. Chem. Soc.* **2008**, *130*, 1830. (c) Wilson, E. F.; Miras, H. N.; Rosnes, M. H.; Cronin, L. *Angew. Chem., Int. Ed.* **2011**, *50*, 3720. (d) Miras, H. N.; Wilson, E. F.; Cronin, L. *Chem. Commun.* **2009**, 1297.
- (27) (a) Ding, J.; Weng, L.-T.; Yang, S. *J. Phys. Chem.* **1996**, *100*, 11120. (b) Solonin, Y. M.; Khlyzhun, O. Y.; Graivoronskaya, E. A. *Cryst. Growth Des.* **2001**, *1*, 473. (c) Santra, Ashok K.; Bird, D. P. C.; Sykes, E. C. H.; Williams, F. J.; Goldoni, A.; Baraldi, A.; Lambert, R. M. *J. Phys. Chem. B* **2001**, *105*, 10062. (d) Topalian, Z.; Niklasson, G. A.; Granqvist, C. G.; Osterlund, L. *ACS Appl. Mater. Interfaces* **2012**, *4*, 672.
- (28) (a) Abdallah, W. A.; Taylor, S. D. *J. Phys. Chem. C* **2008**, *112*, 18963–18972. (b) Peterson, G. W.; Rossin, J. A.; Karwacki, C. J.; Glover, T. G. *J. Phys. Chem. C* **2011**, *115*, 9644–9650. (c) Smirnov, M. Y.; Kalinkin, A. V.; Pashis, A. V.; Sorokin, A. M.; Noskov, A. S.; Kharas, K. C.; Bukhtiyarov, V. I. *J. Phys. Chem. B* **2005**, *109*, 11712–11719. (d) Jia, L.; Song, H.; Li, Q.; Fang, W.; Tang, Y.; Gao, J.; Zhang, P. *Ind. Eng. Chem. Res.* **2008**, *47*, 8888–8893. (e) Zhou, L.; Madix, R. J. *Langmuir* **2010**, *26* (21), 16282–16286. (f) Park, P. W.; Ledford, J. S. *Langmuir* **1996**, *12*, 1794–1799. (g) Nasir, M.; Xi, Z.; Xing, M.; Zhang, J.; Chen, F.; Tian, B.; Bagwasi, S. *J. Phys. Chem. C* **2013**, *117*, 9520–9528. (h) Chen, W.; Li, Y.; Wang, Y.; Wang, E.; Zhang, Z. *Dalton Trans.* **2008**, 865–867. (i) Zhang, J.; Peng, W.; Chen, Z.; Chen, H.; Han, L. *J. Phys. Chem. C* **2012**, *116*, 19182–19190.
- (29) (a) Haraguchi, N.; Okae, T.; Matsuda, Y. *Inorg. Chem.* **1994**, *33*, 1015–1020. (b) Suzuki, K.; Tang, F.; Kikukawa, Y.; Yamaguchi, K.; Mizuno, N. *Angew. Chem., Int. Ed.* **2014**, *53*, 5356–5360. (c) Sadakane, M.; Dickman, M. H.; Pope, M. T. *Inorg. Chem.* **2001**, *40*, 2715–2719.
- (30) (a) Korenev, V. S.; Floquet, S.; Marrot, J.; Haouas, M.; Mbomekalle, I.; Tauelle, F.; Sokolov, M. N.; Fedin, V. P.; Cadot, E. *Inorg. Chem.* **2012**, *51*, 2349–2358. (b) Molina, P. I.; Miras, H. N.; Long, D.-L.; Cronin, L. *Inorg. Chem.* **2013**, *52* (16), 9284. (c) Ibrahim, M.; Xiang, Y.; Bassil, B. S.; Lan, Y.; Powell, A. K.; de Oliveira, P.; Keita, B.; Kortz, U. *Inorg. Chem.* **2013**, *52* (15), 8399. (d) Miras, H. N.; Stone, D.; Long, D.-L.; McInnes, E. J. L.; Kögerler, P.; Cronin, L. *Inorg. Chem.* **2011**, *50*, 8384–8391.
- (31) (a) Jabbour, D.; Keita, B.; Mbomekalle, I. M.; Nadjo, L.; Kortz, U. *Eur. J. Inorg. Chem.* **2004**, 2036. (b) Bi, L.-H.; Wang, E.-B.; Peng, J.; Huang, R.-D.; Xu, L.; Hu, C.-W. *Inorg. Chem.* **2000**, *39*, 671. (c) Bassil, B. S.; Kortz, U.; Tigan, A. S.; ClementeJuan, J. M.; Keita, B.; Oliveira, P.; Nadjo, L. *Inorg. Chem.* **2005**, *44*, 9360. (d) Mbomekalle, I. M.; Keita, B.; Nierlich, M.; Kortz, U.; Berthet, P.; Nadjo, L. *Inorg. Chem.* **2003**, *42*, 5143. (e) Keita, B.; Lu, Y.-W.; Nadjo, L.; Contant, R. *Electrochim. Commun.* **2000**, *2*, 720.